The Impact of Sinusoidal Amplitude on Visualising Thermodynamic Dispersion in Fourier Transformed AC Voltammetry

Alister R. Dale-Evans,[a,b] Nicholas D. J. Yates,[b] Rifael Z. Snitkoff-Sol,[c] Lior Elbaz,[c] Alan M. Bond,†[d] David J. Gavaghan,*[a] Alison Parkin+[b]

Mathematical models of voltammetric experiments commonly contain a singular point value for the reversible potential, whereas experimental data for surface-confined redox-active species is often interpreted to contain thermodynamic dispersion, meaning the population of molecules on the electrode possess a distribution of reversible potential values. Large amplitude ramped Fourier Transformed Alternating Current Voltammetry (FTacV), a technique in which a sinusoidal potential-time oscillation is overlaid onto a linear potential-time ramp, is known to provide access to higher order harmonic components that are largely devoid of non-Faradaic current. Initially, a theoretical study reveals that the use of very large amplitude sinusoidal oscillations reduces the apparent effects of thermodynamic dispersion; conversely, frequency can be varied to change the sensitivity of the measurement to kinetic dispersion. Subsequently, FTacV measurements are used to probe a highly thermodynamically dispersed surface-confined ferrocene derivative attached to a glassy carbon electrode, with amplitudes ranging from 25 to 300 mV and low frequency, which minimises the impact of kinetic dispersion. The results from the experimental study validate the theoretical predictions, demonstrating that we can vary the amplitude in FTacV experiments to tune in and out of thermodynamic dispersion.

Introduction

The electrochemistry of surface-confined redox active moieties is of wide interest in diverse areas of science [1,2] including the biochemical study of electron-transfer proteins and enzymes;[3–5] the chemical interrogation of electrocatalysis related to sensing, oxygen reduction, hydrogen evolution, and the electrochemical optimisation of batteries and fuel cells.[6–13] The utility of the technique in its voltammetric form has been well established and has facilitated key insights.[14]

A quantitative understanding of surface-confined electrode processes requires a comparison of experimental and theoretical data to be undertaken in order to provide estimates of the values of parameters present in the theoretical model. In principle, the theoretical description of an electrode process involving the diffusionless reduction of a surface-confined material, $[\mathrm{Ox}]_{\mathrm{surf}}$, to a surface-confined product, $[\mathrm{Red}]_{\mathrm{surf}}$, as in equation (1), is straightforward.[1,2] Commonly, the electrode reaction is modelled by combining the Nernst equation, if the electron-transfer process is reversible, or the Butler-Volmer equation, if electron-transfer is not reversible, with the time-potential dependent surface concentration of $[\mathrm{Ox}]_{\mathrm{surf}}$ and $[\mathrm{Red}]_{\mathrm{surf}}$.[1,2] When using the Butler-Volmer equation, the important parameters which need to be estimated by extensive, ideally computer-aided, data optimisation procedures are typically the reversible potential (E^0), the charge-transfer rate constant (k^0) at E^0, and, if not known from independent measurements, the surface coverage (Γ).[1,2] Additionally, the charge transfer coefficient, α^0, may be included in the optimisation; however it is often pinned to 0.50.[1,2]

$$[\mathrm{Ox}]_{\mathrm{surf}} + \mathrm{e}^- \rightleftharpoons [\mathrm{Red}]_{\mathrm{surf}} \quad (1)$$

When considering the surface-confined redox system given in reaction (1), the theory is historically described by combining the appropriate model for electron-transfer with a Langmuir isotherm;[15,16] meaning that classically, the following is assumed:[1,15,16]

1. The surface-confined electroactive molecule layer is a monolayer or less.
2. The orientations of surface-confined electroactive molecules are all identical.
3. Surface-confined electroactive molecules do not interact with each other.
4. Variation of the surface chemistry to which the molecules are attached is negligible.
5. Electron-transfer involving surface-confined electroactive molecules only occurs at the electrode.
6. The ratio of the activities of the oxidised and reduced forms of the surface-confined electroactive molecules are given by the ratio of the surface concentrations of $[\mathrm{Ox}]_{\mathrm{surf}}$ and $[\mathrm{Red}]_{\mathrm{surf}}$.

[a] Alister R. Dale-Evans, Prof. David J. Gavaghan*
Department of Computer Science, University of Oxford, Oxford, United Kingdom
*E-mail: david.gavaghan@cs.ox.ac.uk

[b] Alister R. Dale-Evans, Dr. Nicholas D. J. Yates, Prof. Alison Parkin+
Department of Chemistry, University of York, Heslington, United Kingdom
+E-mail: alison.parkin@york.ac.uk

[c] Dr. Rifael Z. Snitkoff-Sol, Prof. Lior Elbaz
Department of Chemistry, Bar-Ilan Center for Nanotechnology and Advanced Materials, Bar-Ilan University, Ramat-Gan 5290002, Israel

[d] Prof. Alan M. Bond
School of Chemistry, Monash University, Clayton, VIC 3800, Australia
†E-mail: alan.bond@monash.edu

These assumptions mean that for the resulting model, the redox activity of all electroactive molecules in a surface-confined voltammetric experiment can be described by a single set of parameter values, i.e. we assume all electroactive molecules have the same E^0, k^0, and α^0 values. However, if any of the assumptions 1-6 are not applicable, the voltammetric experiment cannot be perfectly described by a single set of these parameters.

In practice, surface-confined electrochemical data predicted by the simple model described above almost invariably deviate from experimental behaviour.[17–33] In some cases, this has been ascribed to dispersion which implies there is a need to accommodate in a modified theory a range of values for either one or both of the thermodynamic driving force of the surface-confined molecules (E^0) and the electron-transfer reaction rate (k^0); these two possibilities are known as thermodynamic and kinetic dispersion, respectively. The complications of this so-called 'dispersion' in the analysis of surface-confined voltammetry have been recognised for some time.[17–22,28,29,32–36]

In protein film electrochemistry (PFE), kinetic dispersion has been proposed to originate from the proteins having a range of orientations when confined to an electrode surface.[1,3–5,24,26,32,34,37] The resultant variable distances of the electron-transfer centres to the electrode surface introduces a distribution in k^0 in a manner described by the Marcus distance vs rate relationship,[1] with centres closest to the electrode surface having the highest rate constants for electron-transfer. This can be observed in the k^0 dispersion data in Figure 1 (a) which is from a study of a fluorophore modified copper azurin protein and can be described by a log-Gaussian distribution.[34,36] Similar distributions of k^0 have been observed in metalloenzyme studies, particularly of hydrogenases.[32]

Failure of any of assumptions 1-6 listed above could be separately interpreted to result in kinetic and/or thermodynamic dispersion. This is because any variation in the ground state energy of one molecule versus another would be expected to result in the molecules displaying different electron-transfer energetics. As such, Patil et al[17] have attributed the origin of thermodynamic dispersion in PFE as arising from 'a number of microenvironmental factors such as imperfections in the electrode surface, lateral protein interactions, variant structural perturbation and orientation at the surface, dispersion in the supporting monolayer quality, and associated redox site-electrode coupling'.[17] Indeed, in the dual electrochemical and spectroscopic study of a fluorophore-modified azurin attached to a gold electrode which generated the kinetic dispersion shown in Figure 1 (a), thermodynamic dispersion was also quantified; the dispersion in E values was attributed to changes across the packing of the self-assembled monolayer, and was characterised as Gaussian (Figure 1 (b)).[34,36] Additionally, Palacios et al[38] report a distribution of E^0 values in their studies of single molecules confined to a surface. A recent technique developed by Wright et al.[37], which uses scanning electrochemical cell microscopy to simultaneously observe the surface of an activated electrode and the changes in the local voltammetric response of an attached molecule, may ultimately illuminate the mechanism of thermodynamic dispersion on different electrode surfaces more precisely.

The impact of dispersion on surface-confined voltammetry has been presented for DC,[16] square wave,[39–41] AC,[15] and square-wave voltacoulommetry,[41] and the predicted impact is clearly technique-dependent. The inception of this present study came from the recognition of a strong link between the impact of thermodynamic dispersion and the amplitude of the sine wave superimposed onto the DC ramp in ramped-Fourier Transformed AC Voltammetry (FTacV). The theory and practicalities of FTacV are covered in the literature.[42] Applying a high amplitude sinusoid will also increase the current magnitude; this is par-

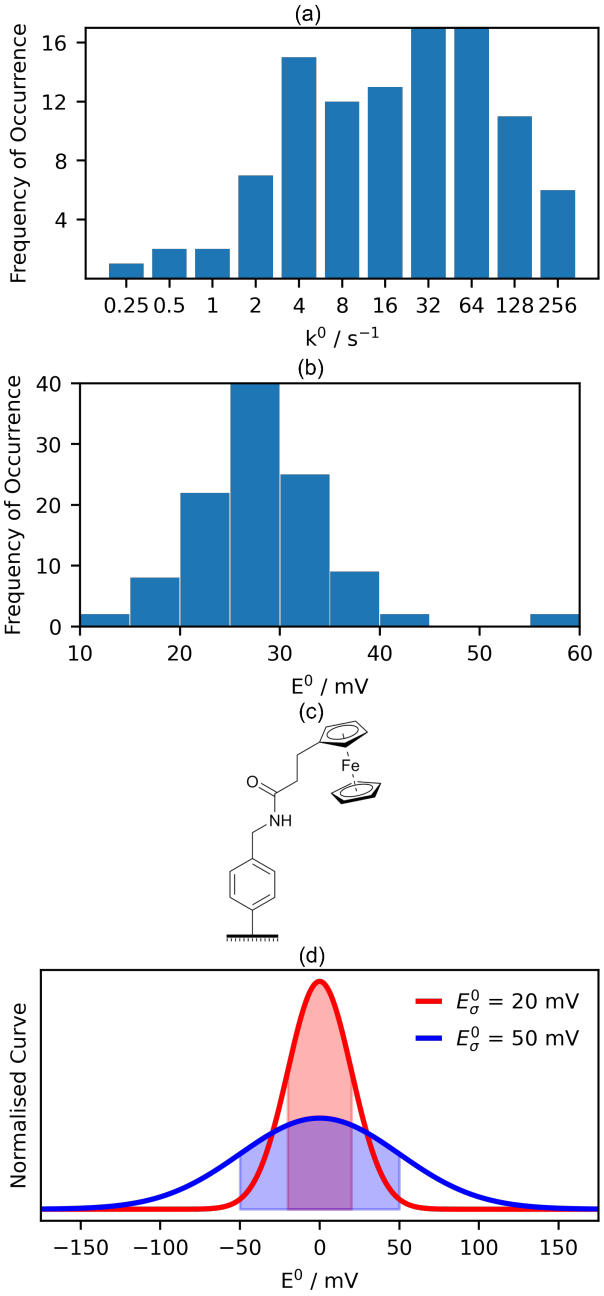

Figure 1. (a) Histogram of the distribution of experimentally determined k^0 values and (b) histogram of the distribution of experimentally determined E^0 values for a surface-confined modified azurin metalloprotein as reported by *Salverda et al.*[36] (note the x-axis in (a) scales to the power of 2).[34,36] (c) N-(benzyl)propan-3-(ferrocenyl)-amide functionalization. (d) Gaussian distributions for thermodynamic dispersion in E^0 centred at 0 mV (E^0_μ). The blue curve represents a high dispersion case, $E^0_\sigma = 50$ mV, and the red curve a low dispersion case, $E^0_\sigma = 20$ mV. The shaded regions encapsulate one standard deviation.

ticularly advantageous for enabling access to Faradaic current in higher-order harmonics.[43] In this work, we demonstrate that varying the amplitude of the applied sine wave in a FTacV experiment can be used to influence sensitivity to thermodynamic dispersion. We first investigate this using simulated experiments before extending to FTacV experimental data gathered at multiple amplitudes for electrode surfaces functionalised with the amide-tethered ferrocene derivative given in Figure 1 (c). A previous study[44] has shown that the surface-confined ferrocene derivative is a high thermodynamic dispersion system.

When considering the amide-tethered ferrocene fuctionalised electrode surface, ideally all the ferrocene moieties should be tethered to the electrode in the same way, so that variation in the distance of these redox active centre and the electrode should be minimised. However, the polished glassy carbon electrode surface to which the ferrocene derivative are attached will not be perfectly smooth; tethering will therefore occur at a range of angles, giving rise to non-idealities and possible kinetic dispersion. Our theoretical study therefore also explores how kinetic dispersion is visualised in FTacV experiments.

Methods

A basic outline of the models used in this work is given here. A detailed write-up can be found in the literature.[23,34]

In FTacV, the input applied potential is a combination of a ramped DC signal $E_{\mathrm{DC}}(\mathrm{t})$ and a sinusoidal AC signal $\Delta E \sin(2\pi f t)$. The DC signal is defined as:

$$E_{\mathrm{DC}}(t) = \begin{cases} E_{\mathrm{start}} + vt, & \text{for } 0 \leq t < t_{\mathrm{rev}} \\ E_{\mathrm{rev}} - v\,(t - t_{\mathrm{rev}})\,, & \text{for } t \geq t_{\mathrm{rev}} \end{cases} \tag{2}$$

$$t_{rev} = \frac{E_{\mathrm{rev}} - E_{\mathrm{start}}}{v}\ , \tag{3}$$

where v is the DC scan rate (i.e. the rate of change of the DC ramp), E_{start} is the initial applied potential, and E_{rev} is the potential of scan direction reversal. Thus the input signal for FTacV may be written as:

$$E(\mathrm{t}) = E_{\mathrm{DC}}(\mathrm{t}) + \Delta E \sin(2\pi f t), \tag{4}$$

where f is the frequency of the applied wave in Hz and is multiplied by 2π to convert to angular radians.

The potential seen by the working electrodes differs from the input applied potential $E(\mathrm{t})$ due to uncompensated resistance R_{u} which arises from the solution between the tip of the reference and the working electrode and resistance of the modified working electrode, resulting in an 'ohmic drop' $(R_{\mathrm{u}} I_{\mathrm{tot}}(\mathrm{t}))$ where I_{tot} is the total current (the sum of the Faradaic and capacitance currents), as defined below. This results in:[1]

$$E_{\mathrm{R}} = E(\mathrm{t}) - I_{\mathrm{tot}}(\mathrm{t}) R_{\mathrm{u}}, \tag{5}$$

where E_{R} denotes the potential corrected for resistance.

In this work, the focus is on the impact of dispersion on the surface-confined fast one-electron reversible reduction reaction given in equation (1). For modelling purposes the reaction is described by Butler-Volmer kinetics with inclusion of ohmic drop. For one-electron reactions, this gives:[1]

$$k^{\mathrm{red}}(t) = k^0 \exp\left(-\frac{\alpha^0 F}{RT}\left[E_{\mathrm{R}}(t) - E^0\right]\right), \tag{6}$$

$$k^{\mathrm{ox}}(t) = k^0 \exp\left((1-\alpha^0)\frac{F}{RT}\left[E_{\mathrm{R}}(t) - E^0\right]\right), \tag{7}$$

where the superscript 0 indicates standard conditions (in instances where experiments are not performed under standard conditions, all these values instead become formal), F is the Faraday constant, R is the universal gas constant, T is the temperature in Kelvin, α^0 is the symmetry factor (also known as the charge transfer coefficient), and $E_{\mathrm{R}}(t)$ is the true (effective) potential seen by the working versus reference electrode at time t.

Assuming a Langmuir isotherm, reaction (1) can be modelled as follows. Initially, we let the proportion of surface-confined species in reduced species (red) be Θ_{red}, and the proportion of surface-confined species in the oxidised state (ox) be Θ_{ox}, with initial conditions $\Theta_{\mathrm{red}} = 1$ and $\Theta_{\mathrm{ox}} = 0$. The Ordinary Differential Equation (i.e. ODE) governing the reaction's behaviour is therefore given by:

$$\frac{\mathrm{d}\Theta_{\mathrm{ox}}}{\mathrm{d}t} = k^{\mathrm{ox}}(1 - \Theta_{\mathrm{ox}}) - k^{\mathrm{red}}\Theta_{\mathrm{ox}}. \tag{8}$$

Note $\frac{\mathrm{d}\Theta_{\mathrm{red}}}{\mathrm{d}t}$ and Θ_{red} are redundant as $\Theta_{\mathrm{red}} = 1 - \Theta_{\mathrm{ox}}$, and are therefore omitted.

The Faradaic current produced by the surface confined system can be modelled as:

$$I_{\mathrm{f}} = FS\Gamma\left(\frac{\mathrm{d}\Theta_{\mathrm{ox}}}{\mathrm{d}t}\right), \tag{9}$$

where F is Faraday's constant, S is the surface area of the electrode, and Γ is the surface coverage in moles per unit area. Since the total current is a combination of the Faradaic and capacitance contributions:

$$I_{\mathrm{tot}} = I_{\mathrm{f}} + I_{\mathrm{c}}, \tag{10}$$

where I_{c} is capacitive or background current, and is given by:

$$I_{\mathrm{c}} = SC_{\mathrm{d}}\frac{\mathrm{d}E_{\mathrm{R}}}{\mathrm{d}t} \tag{11}$$

For experimental systems, FTacV is utilised to filter out background current. For the purpose of the synthetic study capacitance was neglected, i.e. $I_{\mathrm{c}} = 0$.

The approaches to modelling dispersion used in this work are detailed in references[23,34] and are summarised below. When thermodynamic and kinetic dispersion are present, the E^0, k^0, and perhaps α^0 parameters are no longer described by a single value but instead are assumed to draw from probability distributions which capture the degree of dispersion.

If we assume that dispersion is present only on a single parameter, p, modelling may be undertaken by drawing from a probability distribution $\phi(p)$. This distribution leads to a total observed Faradaic current, I_{disp} given by the expectation $E\left[I_{\mathrm{tot}}(t,p)\right]$:

$$I_{\mathrm{disp}} = \int_A I_{\mathrm{tot}}(t,p)\,\phi(p)\,dp \tag{12}$$

In equation (12) A is the range of the integral. Equation (12) may be easily extended for multiple dispersed parameters by multiple integration. In the simulations undertaken in the synthetic data study, thermodynamic dispersion is drawn from the Gaussian distributions displayed in Figure 1 (d) where the standard deviations are 20 or 50 mV and

typically describe the experimentally observed dispersion in E^0 measured for azurin (see Figure 1 (b))[34] and used in a previous simulated data study[23].

When approximating $E[I(t,p)]$ in this work, the Gauss-Hermite quadrature is employed and we therefore assume the underlying distribution $\phi(p)$ is Gaussian. Note the Gauss-Hermite quadrature below is given for a single parameter (i.e. $E[I(t,p)]$), but they can easily be combined for multiple integrals and parameters, such as in equation (12). Integrals of polynomial functions of degree $2n-1$ may be calculated exactly using Guass-Hermite quadrature by discretising the function:

$$\int_{-\infty}^{\infty} \exp\left(-x^2\right) f(x)\,\mathrm{dx} = \sum_{\mathrm{i}=0}^{N_\mathrm{b}} w_\mathrm{i} f(x_\mathrm{i}) \tag{13}$$

For the expectation value of a Gaussian distribution, $E_\mathrm{G}[I(t,p)]$ may be written in the form:

$$E_\mathrm{G}[I(t,p)] = \int_{-\infty}^{\infty} \frac{1}{\sigma\sqrt{2}\pi} \exp\left(\frac{-(p-\mu)^2}{2\sigma^2}\right) I(p,t)\,\mathrm{dp}. \tag{14}$$

where μ and σ are the mean and standard deviation of the Gaussian distribution respectively. Applying the transformation $p = \sigma\sqrt{2}x + \mu$ to equation (14) gives:

$$E_\mathrm{G}[I(t,p)] = \int_{-\infty}^{\infty} \frac{1}{\sqrt{\pi}} \exp\left(-x^2\right) I\left(\sigma\sqrt{2}x + \mu, t\right) \mathrm{dx}, \tag{15}$$

and applying equation (13) to this yields:

$$E_\mathrm{G}[I(t,p)] \approx \sum_{\mathrm{i}=0}^{N_\mathrm{b}} \frac{1}{\sqrt{\pi}} w_\mathrm{i} I\left(\sigma\sqrt{2}x_\mathrm{i} + \mu, t\right). \tag{16}$$

Equation (16) is a Hermite polynomial of degree N_b. x_i and w_i are the weights for the polynomial and are calculated using the Golub-Welsch algorithm.[45,46]

Modelling kinetic dispersion is slightly more complicated, because of the use of a $\log_\mathrm{e}$-Gaussian distribution. However, as a log-Gaussian distribution gives a Gaussian distribution when the log of the distribution is taken (hence the name log-Gaussian), one can simply model a Gaussian distribution and take its antilog, as is done in this work. Therefore a $\log_\mathrm{e}$-normal distribution of $E_{\mathrm{L-N}}[I(t,p)]$ may be modelled by taking the exponential of equation (16), with appropriate values of σ and μ (in this work describing the distribution on k):

$$E_{\mathrm{L-N}}[I(t,p)] \approx \sum_{\mathrm{i}=0}^{N_\mathrm{b}} \frac{1}{\sqrt{\pi}} w_\mathrm{i} I\left(\exp\left(\sigma\sqrt{2}x_\mathrm{i} + \mu\right), t\right). \tag{17}$$

Equation (17) has the added advantage of allowing the relationship of k^0_σ and k^0_μ (σ and μ in equation (17) respectively for the electron-transfer rate constant k^0 i.e. $p = k^0$) to the underlying Gaussian distribution to be seen more intuitively. As is standard for $\log_\mathrm{e}$-Gaussian distributions, k^0_σ and k^0_μ refer to the $\log_\mathrm{e}$ of the values associated with the underlying Gaussian distribution, i.e. a $\log_\mathrm{e}$-Gaussian distribution with $k^0_\sigma = 100\ \mathrm{s}^{-1}$ and $k^0_\mu = 2\ \mathrm{s}^{-1}$ refers to an underlying Gaussian distribution with mean of $\log_\mathrm{e}(100)$ and standard deviation of $\log_\mathrm{e}(2)$; this can be seen in Figure S1.

This model was implemented in Python and thirty-two bins were used for dispersion simulations in this study unless otherwise stated.

Experimental Methods for FTacV Measurements of Surface-Confined Ferrocene

Experimental data were collected using a ferrocene derivative covalently attached to a glassy carbon working electrode as shown in Figure 1 (c). The preparation of the N-(benzyl)propan-3(ferrocenyl)-amide functionalised surface (synthesis and electrode immobilisation strategy) was adapted from the literature,[44,47] and is detailed in the SI.

Experiments on ferrocene-modified electrodes and ferrocene-free 'blank' electrode controls reported in the main paper were conducted in a pH 4.0 aqueous buffer solution consisting of 15 mM each of MES, CHES, HEPES, TAPS, and Na acetate with 2M NaCl supporting electrolyte using a glassy carbon electrode with a geometric surface area of 0.07 cm^{-2}, a scan rate (v) of 40.05 mVs^{-1}, E_start was -350 mV vs SCE, and E_rev 725 mV vs SCE. The applied amplitude, ΔE, covered the range 25 mV to 300 mV in 25 mV increments, and a frequency of ≈8.95 Hz was used (the voltammeter accounts for periodicity by varying the applied frequency slightly when the amplitude is varied, thus the applied frequency varies between 8.941 and 9.015 Hz). Pre-experiment and post-experiment constant potentials of -350 mV were applied for 5 s. A Pt counter electrode and a saturated calomel reference electrode (SCE) were used to complete the three electrode cell arrangement. All electrodes were placed in a water-jacketed all-glass electrochemical cell (in-house design and construction) with a thermostated water-circulator (Grant) used to maintain a temperature of 298 K. Experiments were undertaken under a nitrogen atmosphere in a glove box ($\mathrm{O_2} \leq 50$ ppm), FTacV measurements were conducted using in-house built instrumentation described elsewhere.[43,48] DCV experiments described in the SI were undertaken using the same experimental set-up but with a Ivium compactstat.e potentiostat.

Results and Discussion

Simulated Data Study

We began by exploring the impact of the applied amplitude of FTacV experiments on models containing different amounts of thermodynamic dispersion. Using the theory presented in the Methods section, 8.88 Hz FTacV experiments for a reversible surface-confined single electron-transfer process (given in equation (1)) were simulated with applied amplitudes of 50 mV, 150 mV, 300 mV, and 1000 mV. Simulations were initially completed with and without the presence of thermodynamic dispersion and without the presence of kinetic dispersion; other parameters are as given in Table 1. Note that only Faradaic current is included in these simulations. AC harmonics 1 to 7 derived from the synthetic data obtained with $k^0 = 10^5\ \mathrm{s}^{-1}$ are produced in Figure 2; Figures S2(a) and S3(a) show the equivalent data for a process with a singular k^0 value of $100\ \mathrm{s}^{-1}$. With an experimentally unrealistically large amplitude of 1000 mV, it can be seen that for both the reversible (Figures 2 and S3(a)) and quasi-reversible (Figure S2(a)) cases that the impact of thermodynamic dispersion is negligible in AC harmonics 1 to 7.

Table 1. Modelling parameters used in the simulated data study.

Parameter	Value	Parameter	Value	Parameter	Value
E^0_μ	0.0 mV	E_{start}	-500 mV	E_{rev}	500 mV
f	8.88 Hz	v	22.35 mVs^{-1}	ΔE	50/150/300 mV
S	0.07 cm^{-2}	R_{u}	0.0 Ω	C_{d}	0.0 F cm^{-2}
Γ	1E-10 moles cm^{-2}	α^0	0.5	k^0	100/10^5 s^{-1}
T	298 K	E^0_σ	20/50 mV		

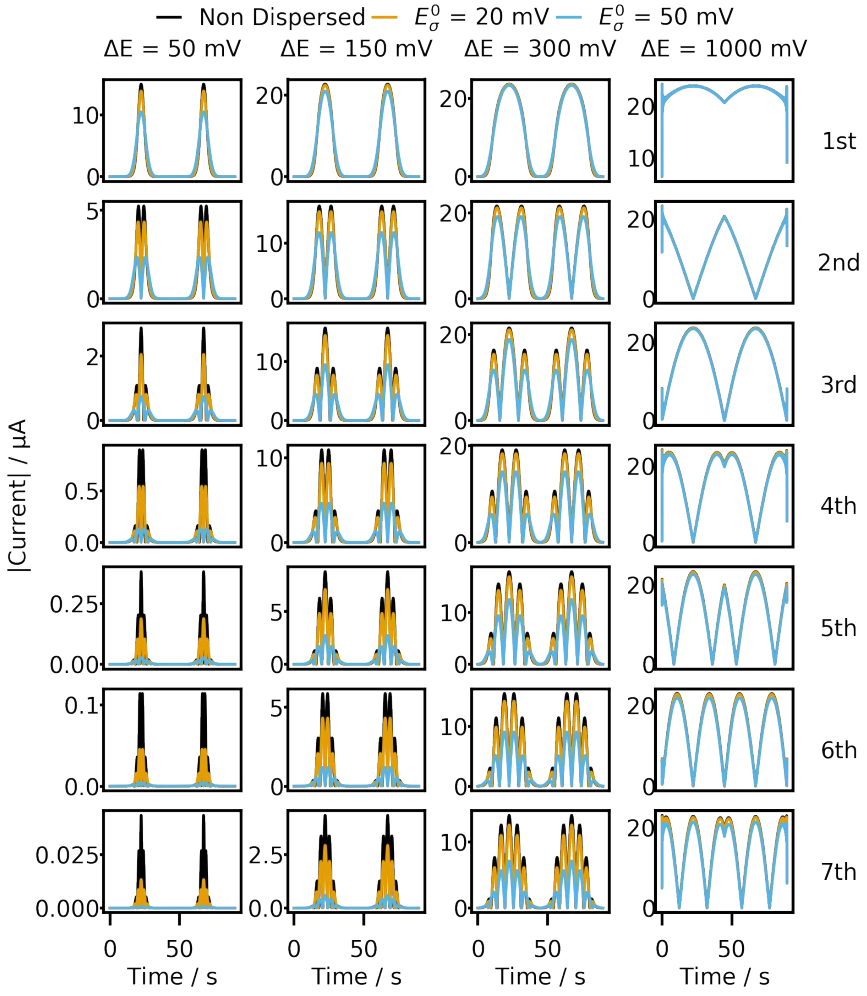

Figure 2. The effect of the amplitude of the sine wave in 8.88 Hz FTacV (top labels) on simulations of harmonics 1-7 (top to bottom) without (non-dispersed, black line) and with thermodynamic dispersion (yellow and blue lines) for a reversible process ($k^0/k^0_\mu = 10^5$ s^{-1}). Parameters that are not explicitly stated are as given in Table 1.

Closer scrutiny of Figure 2, Figure S2(a), and S3(a) reveals that the impact of thermodynamic dispersion increases as the harmonic order increases; and the difference between dispersed and non-dispersed models increases as the applied amplitude of the sine wave of the simulated FTacV experiment decreases (i.e. from right to left across Figure 2 and Figure S2-S3(a)). The origin of the apparent decrease in sensitivity to thermodynamic dispersion with increasing sine wave amplitude can be mathematically understood by considering the proportion of oxidised molecules on the electrode surface (Θ_{ox} see Equation (8)). As the amplitude ΔE becomes larger, the Faradaic signal becomes accessible for a wider range of the applied DC component (or a greater time period) of the applied FTacV protocol (see Figure 3 (a)). In the presence of dispersion, a single value of E^0 is replaced by a distribution of values defined by E^0_μ and E^0_σ, this additionally widens the region of the applied protocol for which Faradaic signal is present. For low thermodynamic dispersion under sufficiently large amplitude, the Faradaic signal range increase caused by dispersion becomes negligible. Furthermore, in the presence of thermodynamic dispersion the larger amplitude ensures a larger proportion of the distribution of E^0 defined by E^0_μ and E^0_σ is accessible within each sinewave oscillation (see Figure 3 (a)) and causes a similar amount of oxidation/reduction as for the non-dispersed case. This is demonstrated in Figure 3 (b), (c), and (d) for ΔE = 50 mV, ΔE = 150 mV, and ΔE = 300 mV respectively; the time period for which the E^0_σ = 0 mV and

E^0_σ = 25 mV simulations overlap can be seen to be significantly increased for the very high amplitude case. An equivalent approach would be to consider the power spectrum; the bandwidth of each individual harmonic narrows with increasing amplitude regardless of dispersion - this is analogous to what we see in the time domain in Figure 2 and Figure 3. This can be understood by considering the contribution of the amplitude term (ΔE) from equation (4) and the effect of dispersion on mid-point potential (E^0) in equations (6) and (7). This also clarifies why the current from the high dispersion model decreases dramatically when simulated for a low amplitude FTacV experiment; in this case, the signal becomes a sum of many sinewaves shifted from one another in the frequency domain.

In the above and following study, a Gaussian distribution of E^0 values was assumed. However, other distributions are plausible. Nevertheless, given this explanation, the impact of all thermodynamic distributions would be minimised given sufficiently large amplitudes due to complete crossing of the distribution being accessible for a larger proportion of the applied protocol.

Simulations were then carried out to explore the impact of applied FTacV amplitude on the appearance of data from models including kinetic dispersion. Figure S2(b) shows that the model is insensitive to kinetic dispersion for a reversible reaction, $k^0_\mu = 10^5$ s^{-1} and f = 8.88 Hz, as one would logically expect because when the timescale of the measurement is slow relative to the kinetics of the reaction the Butler-Volmer kinetics collapse to the Nernst equation, which is devoid of kinetics. In the quasi-reversible case (modelled as $k^0 = 100$ s^{-1} at a frequency of 8.88 Hz) sensitivity to kinetic dispersion is tuned by the applied FTacV amplitude (see Figure S2(c)). Contrasting the simulated effect of thermodynamic dispersion (Figure S2(a)) and kinetic dispersion (Figure S2(c)) under these conditions and across the dispersion ranges explored shows greater amplitude dependence for thermodynamic dispersion. Furthermore, the FTacV frequency can be decreased to minimise sensitivity to kinetic dispersion, this is shown by comparing Figure S2 and S3, when using a frequency of 1 Hz rather than a frequency of 8.88 Hz to probe a process with $k^0 = 100$ s^{-1} the sensitivity to thermodynamic dispersion is not affected (contrast Figure S2(a) and Figure S3(a)) however the sensitivity to kinetic dispersion is significantly decreased (contrast Figure S2(c) and Figure S3(b)) because decreasing the frequency of the experiment has returned the system to equilibrium conditions. Kinetic dispersion was therefore not considered further in this study of amplitude dependence, as sensitivity to kinetic dispersion is better tuned by changing the frequency in a FTacV experiment.

Experimental Study

We now turn our attention to experimental data obtained for the reversible oxidation of the ferrocene derivative N-(benzyl)propan-3(ferrocenyl)-amide confined to a glassy carbon electrode (Figure 1 (c)). The necessary synthesis and electrografting steps are detailed and illustrated in the SI (Figures S4 - S20). On our in-house built potentiostat, the maximum amplitude available is 300 mV. When using such a high amplitude, the DC potential range over which Faradaic current is present is large, as illustrated by the simulation shown in Figure S21. To maximise data usability, it is important to have a region of non-Faradaic current on either side of the Faradaic current regions for two reasons: 1) to separate out the Faradaic signals of the anodic and cathodic sweep of the experiment, and 2) to have a sufficient region free of Faradaic signal to use for a capacitance fitting step if a two-step fitting approach, with capacitance first fitted to the total current in the time domain, is used.[49,50]

Optimisation of the FTacV experimental parameters and buffer system was first carried out to determine the necessary DC ramp range required for 300 mV amplitude FTacV experiments that interrogate the immobilised ferrocene system. When a pH 7.0 buffer system was used, as in the previous immobilised ferrocene FTacV study,[44] substantial oxidative solvent breakdown was observed over the necessary high voltage window (see Figure S22). Therefore, in this work, we have employed a multi-component pH 4.0 buffer to avoid oxidative solvent breakdown. This experimental optimisation highlights that it is not necessarily a trivial matter to carry out FTacV experiments using very large amplitude sine waves.

As is common on carbon based electrodes, a quinone-attributed reversible, non-catalytic Faradaic electron-transfer process is evident in control measurements on blank electrodes, particularly at lower pH (Figure S23).[51–56] These surface reactions have been previously implicated in the anomalous behaviour of redox proteins under slow scan rate cyclic voltammetry conditions.[22] The quinone-attributed signal was of low magnitude relative to the surface confined ferrocene derivative (Figure S20) but is detected in subsequent analysis (discussed in relation with Figures 4, 5, and S23).

Figure 4 shows FTacV data collected for the same surface-immobilised ferrocene 'film' across the amplitude range 25 to 300 mV, with the full data shown in Figure S24. In Figure 4 harmonics 1-3 are resolved using a 'top hat' filter and no downsampling/decimation. Figure 4 clearly confirms that as shown in the synthetic study, amplitude has a substantial impact on the harmonic signals, with improved signal-to-noise ratios being observed in the higher harmonics of higher amplitude experiments. On closer inspection, signs of the impact of dispersion can be seen to decrease with increasing amplitude; for example, the definition of the harmonics lobes can be seen to improve, and a reduction in asymmetry is evident in the relative current magnitude of the peaks obtained from the forwards and backwards DC ramp directions.[23]

To simplify detection of the impact of sine wave amplitude on thermodynamic dispersion, we adopted a heuristic approach to data analysis by carrying out forward simulations using the mathematical model given in the Methods. Initially, we assume an 'ideal' system by which we mean fully reversible, the absence of uncompensated resistance, and no thermodynamic dispersion: $k^0 = 10^5$ s^{-1}, $\alpha^0 = 0.5$, $R_u = 0.0$ Ω, $E^0_\mu = 270.0$ mV vs SCE (equivalent to 510 mV vs SHE, see Figure S25; the estimated mid-point potential was determined by averaging the inflection points of the oxidative and reductive peaks in DCV). Additionally, a linear/Helmholtz capacitance model was utilised ($C_d = 1.5 \times 10^{-5}$ F cm^{-2} was heuristically estimated) for all amplitudes simulated and a surface coverage estimated from DC voltammetry (as detailed in the SI, Figure S26) of $\Gamma = 1.17\text{x}10^{-10}$ mole cm^{-2} was used. Figure 5 (a) shows the experimental data (black line) overlaid with the result of this simulation (orange line) at both: (i) a sinusoidal amplitude of ΔE = 50 mV (left) and (ii) ΔE = 300 mV (right). The total current and harmonics 1 and 2 are shown. The

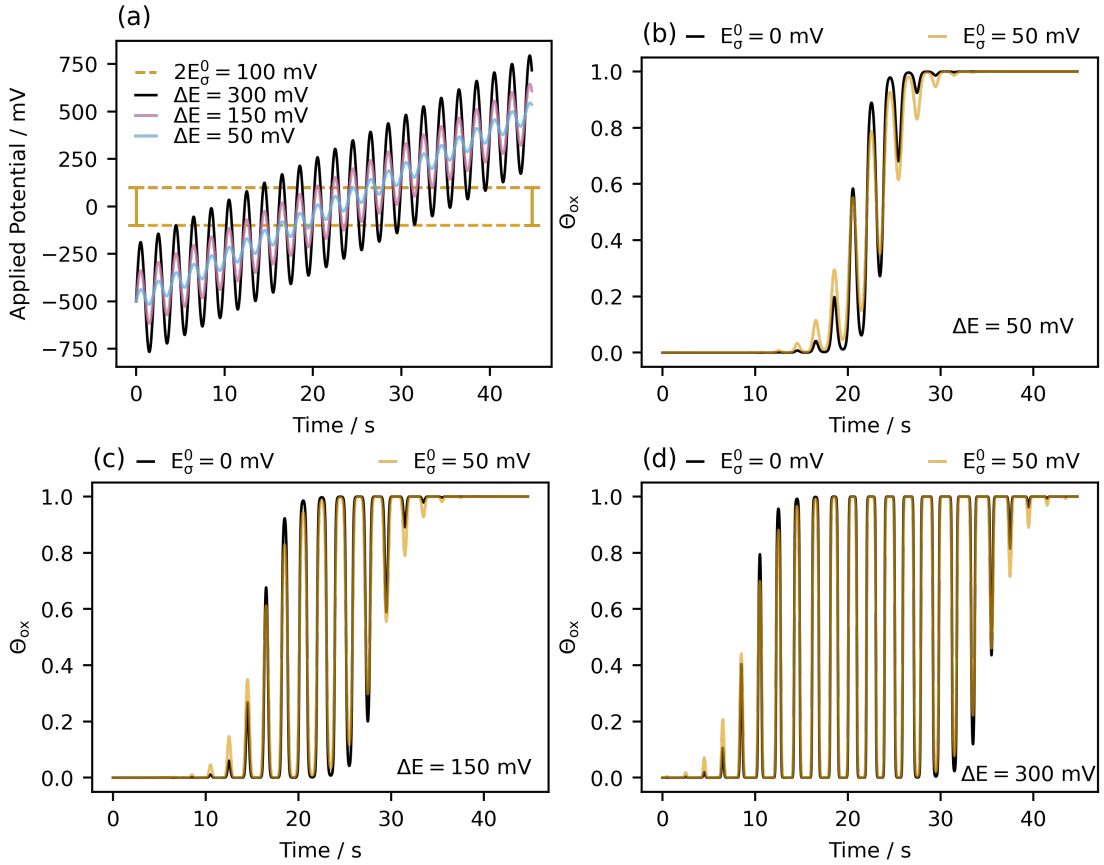

Figure 3. (a) Shows the applied potential vs time of an FTacV experiment with either $\Delta E = 50$ mV (blue), 150 mV (pink), or 300 mV (black), while the yellow outline identifies the potential region containing 95% of the E^0 assuming $E^0_\mu = 0.0$ mV and $E^0_\sigma = 50.0$ mV. The applied protocol uses $f = 0.5$ Hz. (b), (c), and (d) Contrast the proportion of oxidised molecules on the electrode surface (Θ_{ox} see Equation (8)) with (yellow) and without (black) thermodynamic dispersion ($E^0_\sigma = 25.0$ mV) for a reversible process ($k = 10^5$ s^{-1}) without resistance or capacitance, under the three different amplitude conditions of: (b) $\Delta E = 50$ mV, (c) $\Delta E = 150$ mV, and (d) $\Delta E = 300$ mV. All parameters that are not explicitly stated are as given in Table 1.

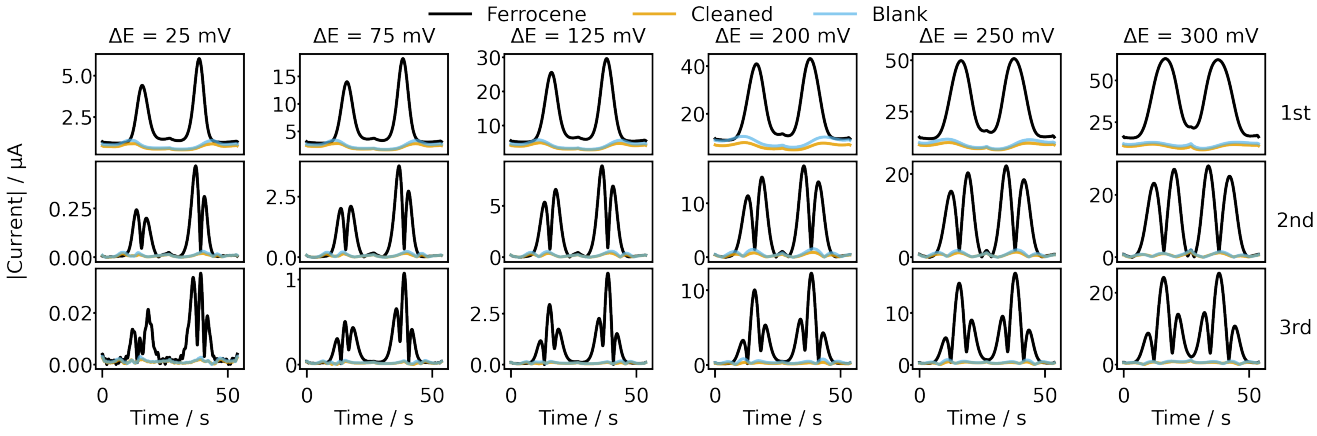

Figure 4. Experimental data for surface confined ferrocene. Top to bottom shows the absolute current magnitude for harmonics 1 to 3. Left to right, the amplitude of the FTacV experiment varies from 25 mV to 300 mV as indicated in the column headings, with data at all amplitudes collected presented in Figure S24. The black lines show measurements made on a ferrocene-functionalised electrode, the orange data was collected post-removal of the ferrocene (by polishing) from the same electrode, and the blue lines show control measurements made on a different, ferrocene free polished glassy carbon electrode which had never undergone any ferrocene surface modification. All parameters used for these experiments are as detailed in the Methods section. Note, a 'top hat' filter has been used, and no decimation or downsampling has been applied in the data processing.

idealised model with no dispersion is clearly not a good fit to the experimental data at either amplitude. The model consistently produces a higher intensity signal than for the experiment at $\Delta E = 50$ mV. In contrast, at $\Delta E = 300$ mV the simulated second harmonic can be seen to be a reasonable match to the experimental data. However, the $\Delta E =$

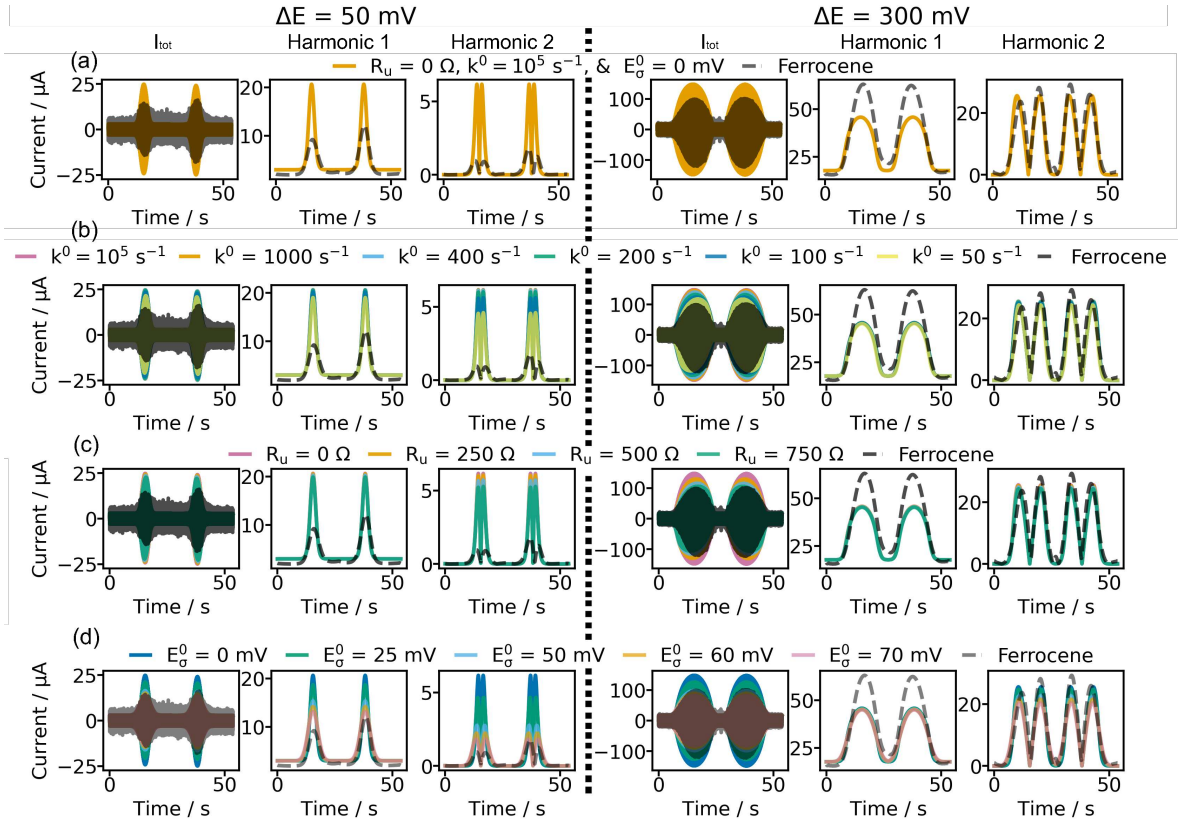

Figure 5. Subplots comparing experimental data (black lines) for an amplitude of 50 mV (column 1-3) and 300 mV (column 4-6) with simulations **(a)** assuming ideal conditions of no resistance, no thermodynamic dispersion, and reversible kinetics, **(b)** varying kinetics, **(c)** varying resistance, **(d)** varying thermodynamic dispersion. Columns 1 and 4 show total current plots, columns 2 and 5 show harmonic 1, and columns 3 and 6 show harmonic 2. No downsampling or decimation has been used for the data presented, and a 'top-hat' filter has been used for harmonic selection. Unless otherwise stated in the legend of **(a)**, **(b)**, **(c)**, and **(d)** the following redox reaction mathematical model parameters were used $k^0 = 10^5$ s^{-1}, $R_u = 0.0$ Ω, $E^0_\mu = 270.0$ mV vs SCE, $E^0_\sigma = 0.0$ mV, $\alpha = 0.5$, $C_{dl} = 1.5 \times 10^{-5}$ F cm^{-2}, and $\Gamma = 1.17 \times 10^{-10}$ mol cm^{-2}. Other model parameters are as defined for the experiment and are given in Section Experimental Methods for FTacV Measurements of Surface-Confined Ferrocene. Note figures in columns 2, 3, 5, and 6 show absolute current magnitude (|current| / μA).

300 mV experiment can be seen to provide more signal than the simulation in the first harmonic. This discrepancy is likely to be at least in part attributable to Faradaic processes related to quinone or other non-ferrocene electroactive species on the polished carbon electrode surface. In FTacV at 8.88 Hz the impact of slow current-generating processes ($k^0 < 10$ s^{-1}) becomes negligible in the 2nd and higher harmonics; Zhang and Bond[57] have theoretically demonstrated that the contribution from catalytic reactions diminishes in the higher harmonics and this has been experimentally validated.[42] Accordingly, we interpret the current in harmonic 1 of the $\Delta E = 300$ mV experiment as arising from contributions from both the immobilised ferrocene and a slow, non-ferrocene electron-transfer process which does not contributed to harmonic 2. As the model used in this work does not account for this additional (putative quinone) electron-transfer process, we cannot capture the enhanced current from this process in harmonic 1 of the simulations.

To better understand the impact of amplitude, we then systematically vary k^0 (Figure 5 (b)), R_u (Figure 5 (c)), and E^0_σ (Figure 5 (d)) to assess their impact on the shape and magnitude of total current and harmonics 1 and 2. From these plots it can be seen that only thermodynamic dispersion mimics the extent of the observed experimental broadening at both amplitudes. R_u can be seen to have more impact at higher amplitudes due to the larger total current response. The impact of decreasing k^0 is very similar to that of increasing R_u, with decreases in current magnitude seen in both cases. Again, within the parameter range examined, broadening to the extent found experimentally is not observed.

The potential separation between the two peaks of the 2nd harmonic in the forward DC ramp direction were measured for the experimental data in Figure 4 and simulations with $k^0 = 10^5$ s^{-1}, $R_u = 0.0$ Ω, $E^0_\sigma = 0.0$ mV, $C_{dl} = 0.0$, and $E^0 = 270.0$ mV. The results are shown in the black and orange plots of Figure 6. This illustrates that the simulated data is considerably narrower than the experimental data at low amplitudes. The simulation of the idealised model becomes approximately the same as the data at $\Delta E = 150$ mV and is wider thereafter, this is because the experiment is not an idealised fully reversible system free of resistance, capacitance, and dispersion, furthermore this is not the only shape-informative metric one would consider when parameterising a model. A perfect model would provide a perfect fit at all amplitudes.

Thermodynamic dispersion was then examined as shown for FTacV experiments with applied amplitudes of 50, 150, and 300 mV in Figure 7. To avoid complications due to putative quinone signals, second and higher order harmon-

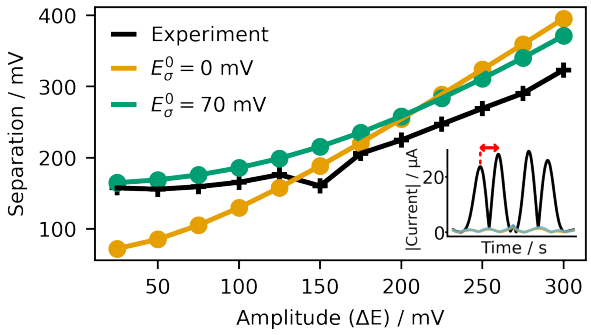

Figure 6. Potential separation between the two peaks of the 2nd harmonic in the forward DC ramp direction (see red arrow in insert) from the experimental data (black) shown in Figure 4 dispersion-free simulations (orange) and simulation featuring thermodynamic dispersion (green) with $E^0_\sigma = 70.0$ mV and all other parameters. For simulations $k^0 = 10^5$ s^{-1}, $R_u = 0.0$ Ω, $E^0_\mu = 0.0$ mV, $C_{dl} = 0.0$ F cm^{-2}, $\Gamma = 1.18$ mole cm^{-2}, and $E^0_\mu = 270$ mV vs SCE.

ics are examined. In this exercise, parameters inferred in prior work[44] were used: $R_U \approx 500$ Ω and $\alpha = 0.5$. In order to observe the impact of thermodynamic dispersion independently of kinetics a value of $k^0 = 10^5$ s^{-1} was chosen (it should be noted that sensitivity to k^0 increases with harmonic order, and so one should not assume all deviation from the idealised model is attributable to thermodynamic dispersion), and as above a surface coverage estimation of 1.17e-10 moles cm^{-2} and $C_d = 1.5 \times 10^{-5}$ F cm^{-2}. All other model parameters were held at the experimental values given in Methods. Figure 7 shows that the experimental findings are consistent with the results of the simulated data study above I) Significant levels of thermodynamic dispersion are needed to mimic harmonics 2 and 3 of the 50 mV amplitude ferrocene data. In contrast, a dispersion-free model approximates harmonics 2 and 3 for the 300 mV amplitude ferrocene experiment. II) For the 300 mV amplitude data, models that included thermodynamic dispersion better mimic the higher harmonics (4-8). This is consistent with the prediction from the theory that higher harmonics are more sensitive to thermodynamic dispersion. III) Signal magnitude and signal-to-noise ratios significantly increase with amplitude. The 8th harmonic of the 300 mV data set has a greater magnitude than the 2nd harmonic of the 50 mV data. Thermodynamic dispersion was then estimated as $E^0_\sigma = 70.0$ mV, as informed by Figure 7, and simulated with $k^0 = 10^5$ s^{-1}, $R_u = 0.0$ Ω, $E^0_\sigma = 0.0$ mV, $C_{dl} = 0.0$, and $E^0 = 270.0$ mV across the range of amplitudes for which experimental data was collected. The potential separation between the two peaks of the 2nd harmonic in the forward DC ramp direction were calculated (green plot, in Figure 6) to compare to the equivalent metric for the experimental data (black) and simulation without dispersion (orange). Thus, Figure 6 further supports the improved fit between the experimental data and a model which includes thermodynamic dispersion.

Conclusion

The technique of large amplitude FTacV, as an alternative to the widely used DCV, has been previously shown to be highly valuable when employed in studies of surface-confined metalloenzymes[44,50,58] catalysts,[6,7,11–13] and other species[8–10,12,13] because Faradaic current contributions from rapid electron-transfer processes can be analysed devoid of contributions from slower processes by isolating the higher order harmonic responses (4th and above) that are accessed in experiments with amplitudes in the region of 150 mV, and frequencies above approximately 5 Hz. This makes it possible to enhance the measurement sensitivity and selectivity. However, previous FTacV studies had still suffered the same "dispersion" problems as other voltammetric measurements of surface-confined species:[17–22,28,29,32–36] generally, it is not possible to accurately simulate the measurements using a minimal mathematical model with a single set of k and E values. This then introduces significant uncertainty in the data analysis: firstly, should a more complicated mathematical model of the reaction include both thermodynamic and kinetic dispersion, or thermodynamic-only, or kinetic-only dispersion? Furthermore, what is the correct form of the parameter distribution which should be included to account for dispersion? Commonly, a Gaussian distribution is utilised, but recent work by Gaudin et al.[59] employing scanning electrochemical cell microscopy showed two distinct activities for hydrogen evolution on a MoS_2 electrode, demonstrating bimodal dispersion is possible. In this paper and previous work,[23] we demonstrated that FTacV becomes insensitive to kinetic dispersion at sufficiently low frequencies. Here, we show that thermodynamic dispersion can be visualised in lower amplitude ($\leq$ 125 mV) FTacV experiments, but it has reduced impact when amplitudes in the 150 to 300 mV region are used.

Importantly, this study has taken a dual theoretical and experimental approach. The simulated data study enabled us to rapidly and simply explore a wide range of different scenarios. Attempting to find experimental systems which had wildly varying electron-transfer rates and a range of different kinetic and thermodynamic dispersion profiles would have been extremely challenging, so the simulations have enormous value in showing how different frequency and amplitude regimes exist in which thermodynamic and kinetic dispersion can be either jointly or separately interrogated. However, because an accurate model does not exist for non-capacitive current, the simulated data was, by necessity, over-simplified. Therefore, it was essential to investigate the theoretical conclusions and extend the work to include surface-immobilised ferrocene experiments. These measurements highlighted key practical challenges that arise when FTacV is attempted across a wide range of different amplitudes. Firstly, there are instrument limitations: while a theoretical study could explore any range of input FTacV amplitudes, we could only apply a maximum of 300 mV. Secondly, every solvent has a limited stability-window. In the ferrocene-experiments, we identified a catch-22 scenario: the optimal buffer pH for maximal solvent stability under high amplitude conditions was the least optimal pH for minimising current contributions from a Faradaic electron-transfer process arising from the glassy carbon electrode (a putative quinine process). Thirdly, the computational simulations do not include noise and fail to highlight the real-world limitations of low amplitude measurements: the substantial drop in signal seen at 50 mV versus 300 mV for the ferrocene system (see Figure 7) means that it would not be trivial to accurately model low amplitude and frequency data to confidently extract thermodynamic dispersion parameters. It

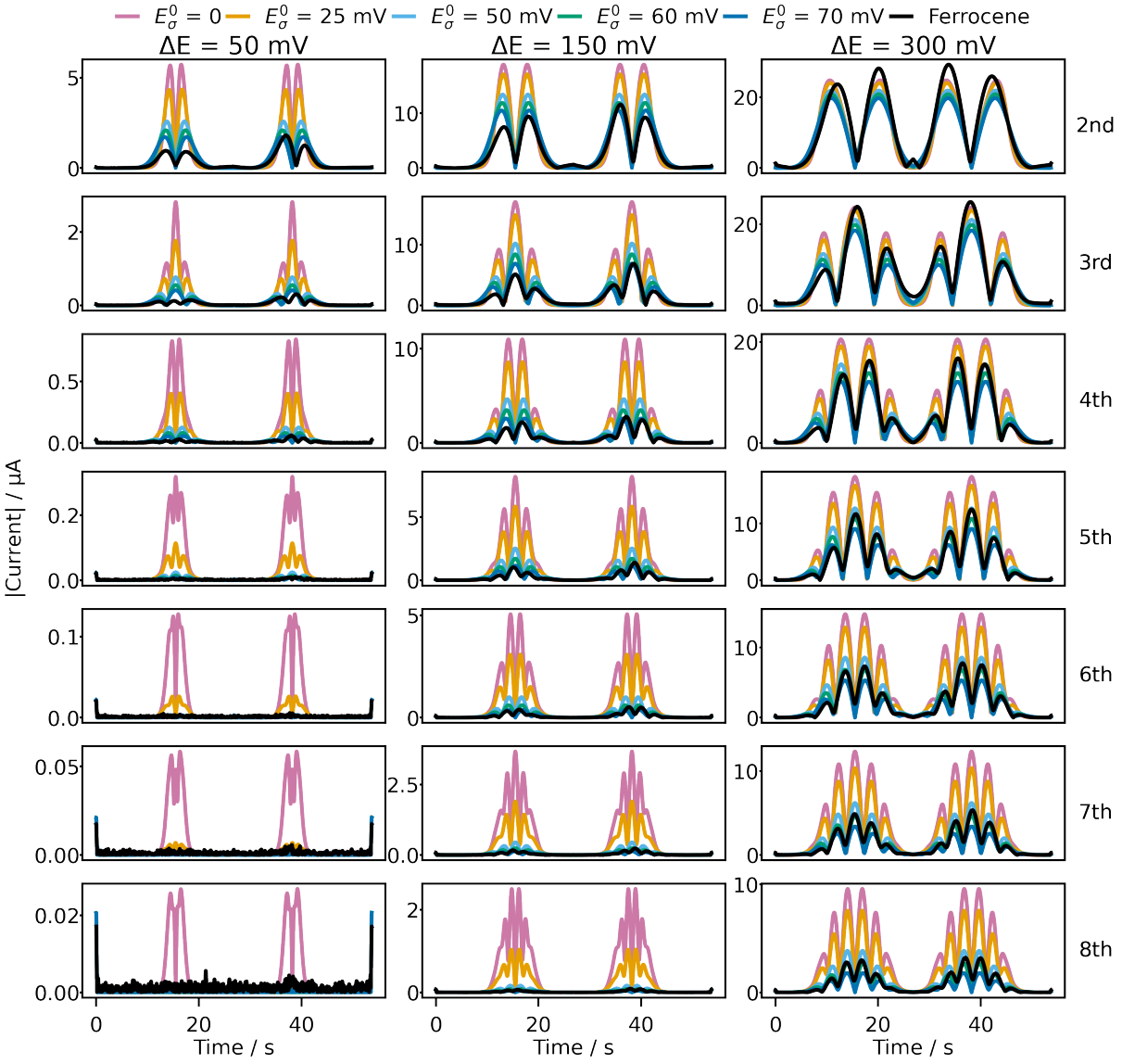

Figure 7. Experimental FTacV data for surface confined ferrocene on a glassy carbon electrode from Figure 4 (black lines) and simulations with (yellow, light blue, green, and dark blue lines) and without (pink lines) thermodynamic dispersion. Top to bottom shows the absolute current magnitude for harmonics 2 to 8. Left to right, the amplitude of the FTacV experiment varies: 50, 150, and 300 mV. The following redox reaction mathematical model parameters were used $k^0 = 10^5$ s^{-1}, $\alpha = 0.50$, $R_u = 500$ Ω, $E^0_\mu = 270.0$ mV vs SCE, and $\Gamma = 1.17 \times 10^{-10}$ mol cm^{-2}. Sixty-four bins were used in the dispersion simulations in this figure. All parameters are as detailed in the Methods section.

is particularly important to note that surface-confined proteins and enzymes have significantly lower electrode-surface coverages due to their macromolecular size. In these systems, the decrease in harmonic signal as a function of decreasing amplitude will be particularly acute and may set a practical signal-to-noise limit that prevents a wide screening of different FTacV amplitudes.

In future work, we will investigate the possibility of using FTacV data collected at a range of amplitudes and frequencies to construct a robust and minimised workflow for confidently and accurately determining both thermodynamic and kinetic dispersion parameters, including the shape of the distributions. Such a quantitative approach was beyond the scope of this work because we will need to include additional measurement techniques (e.g. electrochemical impedance spectroscopy (EIS), and microscopy) to independently verify parameter estimates, and utilise Bayesian statistical analysis to accurately determine when a highly parametrised model is necessary to fit the data versus when a more complex model generates a better fit to the data because it contains more variables (i.e. the model is over-parameterised).

Finally, we note that there are many plausible explanations for the phenomena which we model as thermodynamic dispersion - the exact physicochemical origin has not been determined for our ferrocene films. Further work will therefore also involve understanding how variable amplitude FTacV analysis can help provide insight into thermodynamic and kinetic dispersion on a macroscopic scale that is complementary to microscopic insights into the origins of

this phenomena.

Associated Content

Additional experimental details, supporting DCV plots, and further FTacV simulations are available in the supporting information associated with this article.

Author Contributions

AD-E carried out all the modelling work, synthesis, experimental data collection, and wrote the first draft of the manuscript. NDJY provided expertise in synthesis and voltammetry and helped with the manuscript. RS and LE first noticed an apparent connection between thermodynamic dispersion and the amplitude of the sine wave in ramped-Fourier Transformed AC Voltammetry. AMB, DJG, and AP all contributed to the design of the project and the writing of the final paper.

Acknowledgements

This work was supported by funding from the Biotechnology and Biological Sciences Research Council (UKRI-BBSRC, grant number BB/T008784/1) which AD-E gratefully acknowledges. AMB thanks the Australian Research Council Discovery Program for their support (grant DP 210100606). AP, DG, and NDJY gratefully acknowledge UKRI Horizon Europe Guarantee for their ongoing support (grant code EP/X027724/1).

AD-E would like to express warm thanks to Julia Walton for accommodating the experimental component of this work, and the wider Parkin group for their hospitality.

Conflict of Interest

No conflicts of interest to declare.

Data Availability Statement

The data that support the findings of this study are available in the following repository: https://github.com/alisterde/impact_of_amplitude

Keywords: Electrochemical analysis • Surface-confined ferrocene • Large amplitude Fourier transform voltammetry • Thermodynamic dispersion • Sinusoidal amplitude

References

[1] A. J. Bard, L. R. Faulkner, H. S. White, *Electrochemical methods: fundamentals and applications*, John Wiley & Sons **2022**.
[2] R. G. Compton, C. E. Banks, *Understanding voltammetry*, World Scientific **2011**.
[3] J. A. Cracknell, K. A. Vincent, F. A. Armstrong, *Chemical reviews* **2008**, *108*, 2439.
[4] F. A. Armstrong, H. A. Heering, J. Hirst, *Chemical Society Reviews* **1997**, *26*, 169.
[5] R. M. Evans, B. Siritanaratkul, C. F. Megarity, K. Pandey, T. F. Esterle, S. Badiani, F. A. Armstrong, *Chemical Society Reviews* **2019**, *48*, 2039.
[6] Y. Zhang, L. Chen, F. Li, C. D. Easton, J. Li, A. M. Bond, J. Zhang, *ACS Catalysis* **2017**, *7*, 4846.
[7] L. Chen, F. Li, C. L. Bentley, M. Horne, A. M. Bond, J. Zhang, *ChemElectroChem* **2017**, *4*, 1402.
[8] S.-X. Guo, Y. Liu, A. M. Bond, J. Zhang, P. E. Karthik, I. Maheshwaran, S. S. Kumar, K. L. N. Phani, *Physical Chemistry Chemical Physics* **2014**, *16*, 19035.
[9] Y. Zhang, A. N. Simonov, J. Zhang, A. M. Bond, *Current Opinion in Electrochemistry* **2018**, *10*, 72.
[10] D. A. Bograchev, Y. M. Volfkovich, S. Martemianov, *Journal of Electroanalytical Chemistry* **2023**, page 117322.
[11] R. Z. Snitkoff-Sol, A. Friedman, H. C. Honig, Y. Yurko, A. Kozhushner, M. J. Zachman, P. Zelenay, A. M. Bond, L. Elbaz, *Nature Catalysis* **2022**, *5*, 163.
[12] B. E. Conway, *Electrochemical supercapacitors: scientific fundamentals and technological applications*, Springer Science & Business Media **2013**.
[13] C.-Y. Lee, A. M. Bond, *Analytical chemistry* **2009**, *81*, 584.
[14] A. M. Bond, *Broadening electrochemical horizons: principles and illustration of voltammetric and related techniques*, Oxford University Press on Demand **2002**.
[15] E. Laviron, *Journal of Electroanalytical Chemistry and Interfacial Electrochemistry* **1979**, *97*, 135.
[16] E. Laviron, *Journal of Electroanalytical Chemistry and Interfacial Electrochemistry* **1979**, *101*, 19.
[17] A. V. Patil, J. J. Davis, *Journal of the American Chemical Society* **2010**, *132*, 16938.
[18] M. J. Honeychurch, G. A. Rechnitz, *Electroanalysis: An International Journal Devoted to Fundamental and Practical Aspects of Electroanalysis* **1998**, *10*, 285.
[19] M. J. Honeychurch, G. A. Rechnitz, *Electroanalysis: An International Journal Devoted to Fundamental and Practical Aspects of Electroanalysis* **1998**, *10*, 453.
[20] S. W. Feldberg, I. Rubinstein, *Journal of electroanalytical chemistry and interfacial electrochemistry* **1988**, *240*, 1.
[21] J. Hirst, F. A. Armstrong, *Analytical chemistry* **1998**, *70*, 5062.
[22] L. J. Jeuken, F. A. Armstrong, *The Journal of Physical Chemistry B* **2001**, *105*, 5271.
[23] H. O. Lloyd-Laney, M. J. Robinson, A. M. Bond, A. Parkin, D. J. Gavaghan, *Journal of Electroanalytical Chemistry* **2021**, *894*, 115204.
[24] V. Fourmond, C. Baffert, K. Sybirna, T. Lautier, A. Abou Hamdan, S. Dementin, P. Soucaille, I. Meynial-Salles, H. Bottin, C. Léger, *Journal of the American Chemical Society* **2013**, *135*, 3926.
[25] V. Fourmond, C. Léger, *Current Opinion in Electrochemistry* **2017**, *1*, 110.
[26] O. Vodeb, A. Lončar, M. Bele, A. Hrnjić, P. Jovanovič, M. Gaberščck, N. Hodnik, *Electrochimica Acta* **2023**, *464*, 142882.
[27] J. Cassidy, W. Breen, A. McGee, T. McCormacx, M. Lyons, *Journal of Electroanalytical Chemistry* **1992**, *333*, 313.
[28] R. A. Clark, E. F. Bowden, *Langmuir* **1997**, *13*, 559.
[29] G. K. Rowe, M. T. Carter, J. N. Richardson, R. W. Murray, *Langmuir* **1995**, *11*, 1797.
[30] C. E. Chidsey, C. R. Bertozzi, T. Putvinski, A. Mujsce,

Journal of the American Chemical Society **1990**, *112*, 4301.
[31] W. R. Fawcett, *Journal of Electroanalytical Chemistry* **1994**, *378*, 117.
[32] C. Léger, A. K. Jones, S. P. Albracht, F. A. Armstrong, *The Journal of Physical Chemistry B* **2002**, *106*, 13058.
[33] A. Patil, J. Davis, *Coordination chemistry reviews* **2011**, *255*, 1970.
[34] G. P. Morris, R. E. Baker, K. Gillow, J. J. Davis, D. J. Gavaghan, A. M. Bond, *Langmuir* **2015**, *31*, 4996.
[35] Z. Zhang, J. F. Rusling, *Biophysical chemistry* **1997**, *63*, 133.
[36] J. M. Salverda, A. V. Patil, G. Mizzon, S. Kuznetsova, G. Zauner, N. Akkilic, G. W. Canters, J. J. Davis, H. A. Heering, T. J. Aartsma, *Angewandte Chemie International Edition* **2010**, *49*, 5776.
[37] I. R. Wright, L. F. Gaudin, L. L. Martin, C. L. Bentley, *Electrochimica Acta* **2023**, *471*, 143362.
[38] R. E. Palacios, F.-R. F. Fan, J. K. Grey, J. Suk, A. J. Bard, P. F. Barbara, *Nature Materials* **2007**, *6*, 680.
[39] R. Gulaboski, V. Mirčeski, I. Bogeski, M. Hoth, *Journal of Solid State Electrochemistry* **2012**, *16*, 2315.
[40] V. Mirceski, R. Gulaboski, M. Lovric, I. Bogeski, R. Kappl, M. Hoth, *Electroanalysis* **2013**, *25*, 2411.
[41] J. Gonzalez, A. Molina, *Journal of Solid State Electrochemistry* **2013**, *17*, 537.
[42] N. G. Baranska, B. Jones, M. R. Dowsett, C. Rhodes, D. M. Elton, J. Zhang, A. M. Bond, D. Gavaghan, H. O. Lloyd-Laney, A. Parkin, *ACS Measurement Science Au* **2024**.
[43] A. M. Bond, N. W. Duffy, S.-X. Guo, J. Zhang, D. Elton, *Analytical chemistry* **2005**, *77*, 186.
[44] H. O. Lloyd-Laney, N. D. Yates, M. J. Robinson, A. R. Hewson, J. D. Firth, D. M. Elton, J. Zhang, A. M. Bond, A. Parkin, D. J. Gavaghan, *Analytical Chemistry* **2021**, *93*, 2062.
[45] G. H. Golub, J. H. Welsch, *Mathematics of computation* **1969**, *23*, 221.
[46] A. Gil, J. Segura, N. M. Temme, *Numerical methods for special functions*, SIAM **2007**.
[47] N. D. Yates, M. R. Dowsett, P. Bentley, J. A. Dickenson-Fogg, A. Pratt, C. F. Blanford, M. A. Fascione, A. Parkin, *Langmuir* **2019**, *36*, 5654.
[48] A. M. Bond, D. Elton, S.-X. Guo, G. F. Kennedy, E. Mashkina, A. N. Simonov, J. Zhang, *Electrochemistry Communications* **2015**, *57*, 78.
[49] H. Adamson, M. Robinson, P. S. Bond, B. Soboh, K. Gillow, A. N. Simonov, D. M. Elton, A. M. Bond, R. G. Sawers, D. J. Gavaghan, et al., *Analytical chemistry* **2017**, *89*, 1565.
[50] A. R. Dale-Evans, M. J. Robinson, H. O. Lloyd-Laney, D. J. Gavaghan, A. M. Bond, A. Parkin, *Frontiers in Chemistry* **2021**, *9*, 424.
[51] M. A. Fryling, J. Zhao, R. L. McCreery, *Analytical Chemistry* **1995**, *67*, 967.
[52] P. Chen, M. A. Fryling, R. L. McCreery, *Analytical Chemistry* **1995**, *67*, 3115.
[53] C. A. Thorogood, G. G. Wildgoose, J. H. Jones, R. G. Compton, *New Journal of Chemistry* **2007**, *31*, 958.
[54] C. A. Thorogood, G. G. Wildgoose, A. Crossley, R. M. Jacobs, J. H. Jones, R. G. Compton, *Chemistry of Materials* **2007**, *19*, 4964.
[55] R. L. McCreery, *Chemical reviews* **2008**, *108*, 2646.
[56] K. Chaisiwamongkhol, C. Batchelor-McAuley, R. G. Palgrave, R. G. Compton, *Angewandte Chemie* **2018**, *130*, 6378.
[57] J. Zhang, A. M. Bond, *Journal of Electroanalytical Chemistry* **2007**, *600*, 23.
[58] H. Adamson, A. M. Bond, A. Parkin, *Chemical Communications* **2017**, *53*, 9519.
[59] L. F. Gaudin, I. R. Wright, T. R. Harris-Lee, G. Jayamaha, M. Kang, C. L. Bentley, *Nanoscale* **2024**, *16*, 12345.

Entry for the Table of Contents

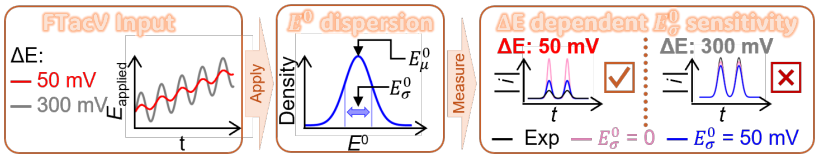

Experimental data for surface-confined redox-active species is often modelled with thermodynamic dispersion. Considering the experimental design of large amplitude ramped Fourier Transformed Alternating Current Voltammetry (FTacV) using a dual theoretical and experimental approach reveals that varying experimental sinusoidal amplitude may be used to tune in and out of thermodynamic dispersion.